Compressive fracture aspect of thick quasi-isotropic carbon fiber reinforced plastic laminates

Keita Goto[a,*], Masahiro Arai[a], Yuki Kano[a], Eiichi Hara[b], Takashi Ishikawa[c]

[a]*Department of Aerospace Engineering, Nagoya University,*
Furo-cho, Chikusa-ku, Nagoya, 464–8603, Japan
[b]*Aeronautical Technology Directorate, Japan Aerospace Exploration Agency,*
6–13–1 Osawa, Mitaka, 181–0015, Japan
[c]*National Composites Center Japan, Nagoya University,*
Furo-cho, Chikusa-ku, Nagoya, 464–8603, Japan

Abstract

The compressive fracture aspect for the thick quasi-isotropic carbon fiber reinforced plastic (CFRP) laminates was investigated using a high-speed camera to clarify the progress of the brooming fracture. The compressive fracture types of the laminates could be classified into two groups, i.e., the fractures initiating from the innermost 0° ply and those initiating from the fixed sections of the specimen. The standard deviation of the compressive strength for the innermost 0° ply-initiated fracture type was larger than that for the fixed-section fracture type, although the average compressive strengths for each fracture mode were similar. The initial fracture in the innermost 0° ply was caused by the microbuckling of the fibers. The numerical results demonstrated a considerable out-of-plane shear stress around the free edges of the specimen, especially for the innermost 0° ply. Such a shear stress is thought to cause the microbuckling at the innermost 0° ply, with the crack

*goto@nuae.nagoya-u.ac.jp

subsequently propagating toward the outer plies of the specimen. The compressive strength of the innermost 0° ply was an important factor affecting the fracture behavior of the thick quasi-isotropic CFRP laminates.

Keywords: A. Carbon fibres, A. Polymer-matrix composites (PMCs), B. Fracture, B. Strength, High-speed images

1. Introduction

Carbon fiber reinforced plastics (CFRPs) are increasingly used in primary parts of aeronautical and aerospace structures. Material tests and component structural tests of composite structures are required and performed in aircraft-development programs. CFRPs exhibit a complex fracture behavior, including transverse cracks, interlaminar delamination, and fiber breaking. In particular, the compressive strength in the fiber direction is approximately 30–40% lower than the tensile strength owing to the microbuckling of the fibers [1, 2]. It is important to clarify the fracture process of CFRPs and its mechanism in the coupon-specimen scale, especially for compressive fracture, from the viewpoint of safety design of CFRP structures.

The previous studies regarding the compressive fracture of CFRPs were primarily focused on the kink band fracture. This is the typical compressive fracture mode for unidirectional CFRP laminates subjected to compressive loads in the fiber direction. The kink band fracture is caused by local buckling of the fibers. The shear yielding of the matrix resin occurs at first due to an initial fiber misalignment. Subsequently, the microbuckling of the fibers occurs because the restriction of the fiber's bending deformation is weakened, which is followed by the final fracture of the CFRP laminates. Therefore, the

2

nonlinear behavior of the matrix resin under shear loads and initial misalignment angles of the fibers are considered to affect the compressive strength of the CFRP laminates significantly. Some well-known theoretical criteria for the compressive strength of the CFRP laminates exist; e.g., the kink band model [1] and the microbuckling model [2]. Furthermore, advanced or combined compressive fracture models based on these criteria have been proposed [3, 4, 5, 6]. In recent years, quantification methods for fiber misalignment in the CFRP laminates [7, 8, 9, 10, 11] have been proposed as visualization and image processing technologies advance. Further improvements in the prediction of the compressive strength of the CFRP laminates can be expected using these modeling methods, which are based on actual laminates.

However, thin laminates were targeted in the studies mentioned above and knowledge of the compressive fracture behavior of thick CFRP laminates is still insufficient [12, 13]. Thick quasi-isotropic CFRP laminates are generally used in actual structures. It is extremely important to estimate the ultimate strength of CFRP structures accurately, especially in the safety design of aircraft, owing to severe design limitations. However, evaluating the compressive fracture behavior is difficult because both the compressive strength and the fracture mechanism change depending on the thickness of the laminates. It is well known that various fracture modes can occur for the quasi-isotropic CFRP laminates. In particular, a characteristic fracture aspect as shown in Fig. 1, which is known as "brooming fracture," can be observed for the thick quasi-isotropic CFRP laminates subjected to a compressive load [13, 14]. Few investigations for the brooming fracture based on experimental or analytical results have been reported. Therefore, evaluat-

ing the compressive strength and determining the fracture mechanism of the thick quasi-isotropic CFRP laminates are highly demanded in the aerospace industry.

It is crucial to observe the fracture process of the laminates in detail to better understand the mechanism of compressive fracture. It is well known that premature and catastrophic fractures occur during compressive tests of CFRP laminates; the fracture process of the CFRP laminates has been investigated primarily based on fractography. The dominant fracture modes in each fractured area can be surmised from the results of fractography. Typical fracture surfaces of the CFRP laminates under tensile, compressive, shear and bending loads have been reported [15, 16, 17, 18, 19]. Jumahat et al. observed a bending fracture surface at the kink band and calculated the kink band angle as $\beta = 10°$–$25°$ from the lateral surface observation [3]. Although the fracture starting point and fracture process in the laminates are difficult to estimate, it was proposed that the origin of the compressive fracture tended to occur at the free edges of the specimen because the restriction of the fiber's deformation by the matrix was weakened [20]. In addition, the in-situ observations of kink band generation using X-ray computed tomography and the special-shaped specimens have been performed in recent years [21, 22], and it has been reported that the kink band originated from one side of the free edges of the specimen and subsequently propagated toward the inside. Therefore, the compressive fracture process of the CFRP laminates can be discussed broadly by observing the occurrence and the propagation of the fracture at the free edges of the specimen.

Meanwhile, the compressive tests of CFRP laminates are inherently dif-

4

ficult. Buckling and end fracture of the specimen often occur in the compressive tests using coupon specimens. To avoid these difficulties, various standard tests have been proposed for the compressive tests of the CFRP laminates. The standard compressive tests can be classified broadly into two groups depending on the compressive loading method used on the specimen. One is the shear-loading compression method, for example, ASTM D3410 (ITTRI method) [23], which induces a compressive load onto the specimen through a shear load at fixed areas of the specimen. The other is the end-loading compression method, for example, SRM 1R-94 [24] and ASTM D695 [25], which induces a compressive load through the specimen ends directly. In addition, the combined-loading compression method, which is a combination of the shear- and end-loading methods, such as ASTM D6641 (CLC method) [26] and NAL-II method [27], has been proposed as well. The fixtures used in these standard tests involve large support rods or sleeves to prevent the specimen from buckling. Thus, it is difficult to capture the images of the compressive fracture process during these tests because most of the specimen is covered by the fixtures.

In the present study, the fracture aspect of the CFRP laminates under compressive tests was investigated using a high-speed camera to clarify the progress of the brooming fracture. The 64-ply quasi-isotropic CFRP specimens were evaluated in the present study. For the compressive tests, an alternative compressive test fixture was developed enabling the capture of high-speed images. From the captured images, the fracture types of the specimens were classified; thereafter the initiation and progress of compressive fracture were considered. In addition, the dominant aspect regarding

the origin of the brooming fracture is discussed based on the observations of fractured surfaces and the numerical considerations obtained using a finite element method (FEM).

2. Experimental procedure

2.1. CFRP specimen

The carbon fiber/epoxy unidirectional CFRP prepregs T800S/#3900-2B (Toray Industries, Inc.) were used in this study. The 64-ply quasi-isotropic CFRP laminates $[45°/0°/-45°/90°]_{8S}$, where S denotes the symmetry of the stacking sequence of the laminate, were made in an autoclave. The average thickness of the specimens was 12.35 mm. The laminates were cut into 100-mm long and 25-mm wide as indicated in Fig. 2. In Fig. 2, the X-, Y-, and Z-directions coincide with the longitudinal, transverse, and thickness directions of the specimen, respectively. $0°$ of the fiber orientation was defined relative to the X-direction of the specimen. Biaxial strain gages were glued at the centers of both sides of the specimen.

2.2. Testing method

The schematics of the uniaxial compressive test is shown in Fig. 3. The 250-kN universal material testing machine INSTRON 5985 was used. The cross-head rate was specified to 1.0 mm/min based on JIS K7076 standard. The original compressive test fixture shown in Fig. 4 was used to capture high-speed images of compressive fracture of the specimen. The test fixture was developed referring to the NAL-II test fixture [27]. The upper side of the fixture can only slide in the loading direction, thereby restricting the

6

bending deformation of the specimen. The specimen is fixed by the retainers and a compressive load is applied through both ends of the specimen, which is the same as the NAL-II test fixture. The fixed sections were 35-mm areas of the top and bottom of the specimen and the gage length was 30 mm. The fastening torque of bolts was set as 3.0 N·m to avoid specimen fracture at the fixed sections. In addition, lubricant was applied on the fixed sections to reduce friction. From the results, it was confirmed that the similar stress-strain curves and compressive strengths can be obtained when comparing the original test fixture used in this study with the NAL-II test fixture.

The fracture process of the quasi-isotropic CFRP specimen during the compressive test was observed using the Hyper Vision HPV-X (Shimadzu Corp.) high-speed camera. The time interval for the high-speed imaging was set as 8 μsec. The number of frames was 256 and therefore the total imaging time was 2040 μsec. The image size was 400×250 pixels. In addition, the metal-halide lamp HVC-SL (Photron Ltd.) and white cardboard were used as a light source and a reflector, respectively. In this study, an aluminum ribbon was used to generate the trigger signal for the high-speed camera when catastrophic fracture occurred in the specimen (Fig. 3) [28]. Electric current flowed to the aluminum ribbon and the trigger signal was generated by cutting the ribbon.

3. Experimental results and discussion

3.1. Uniaxial compressive tests

The representative stress-strain curves of the 64-ply quasi-isotropic CFRP specimen obtained from the uniaxial compressive tests are shown in Fig. 5.

Here, the compressive stress and strain are indicated with a negative sign. The legends, FX, FY, BX, and BY, coincide with the strain gages shown in Fig. 2. The longitudinal compressive and transverse tensile strains increase as the compressive load increases and nonlinear behavior is exhibited in the high compressive-stress region.

The averages and standard deviations of the Young's modulus, compressive strength, and fracture strain of the 64-ply quasi-isotropic CFRP specimens obtained from 44 specimens are shown in Table 1. Here, Yokozeki et al. performed the uniaxial compressive tests of the unidirectional and quasi-isotropic CFRP laminates based on a modified SRM 1R-94 standard; they reported that the averaged compressive strength and fracture strain of the 16-ply quasi-isotropic laminates made of the same T800S/#3900-2B prepregs were 669 MPa and 1.68, respectively [6]. Although the compressive strength of the CFRP laminates varies depending on the compressive test methods, it has been reported that the compressive strength of the quasi-isotropic CFRP laminates obtained by SRM 1R-94 standard is similar to that obtained by NAL-II method [27]. Therefore, it can be considered that the compressive strength and fracture strain of the quasi-isotropic CFRP laminates tend to decrease as the number of plies increases.

3.2. High-speed imaging of compressive fracture

The compressive fracture process of the quasi-isotropic CFRP specimen was analyzed based on the results of high-speed imaging. The high-speed imaging of the compressive fracture was successful in 23 samples among 44 specimens. From the captured images, the compressive fracture types of the quasi-isotropic CFRP specimen can be classified as follows:

8

Type-A: pure innermost $0°$ ply-initiated fracture type The initial fracture occurred at the innermost $0°$ ply of the specimen and propagated in the thickness direction.

Type-B: innermost $0°$ ply-initiated fracture type The initial failure occurred at the outer plies of the specimen, but the final fracture was triggered by a fracture on the innermost $0°$ ply of the specimen.

Type-C: fixed-section fracture type The initial fracture occurred at the outer plies and formed the originating point for the specimen entire fracture.

The histories of these fracture types obtained from the high-speed images are shown in Figs. 6-8. In these figures, 0 μsec is set as the time when the initial fracture of the laminate is observed in the captured images.

In the type-A fracture (Fig. 6), the initial compressive fracture occurred at the innermost $0°$ ply of the specimen and propagated along the loading direction (X-direction). Next, the outer plies began to bend and fracture with fibers breaking and interlaminar delamination occurred in the thickness direction (Z-direction) on one side of the specimen. Subsequently, the fracture propagated to the other side of the specimen. Finally, the specimen was fractured completely and a compressive load reduced significantly.

In the type-B fracture (Fig. 7), the initial compressive failure was observed at the outer plies of the specimen around the fixed sections and a compressive load decreased slightly. This was caused by the stress concentration owing to the restriction in deformation by the fixture. However, the final fracture of the specimen was initiated from micro damage at the inner-

most $0°$ ply and the trigger signal was generated. Subsequently, a similar process to the type-A fracture was observed, but the total time from the occurrence of the initial failure at the outer plies to the final fracture was longer than that of the type-A fracture.

By contrast, for the type-C fracture (Fig. 8), the initial fracture occurred at the outer plies of one side of the specimen; subsequently, fracture with fibers breaking propagated from the outer to the inner plies of the specimen.

From the experimental results and the high-speed images, the averages and standard deviations of Young's modulus, compressive strength, and fracture strain for each compressive fracture type are listed in Table 2. The (pure) innermost $0°$ ply-initiated fracture type (type-A and type-B fractures) constituted a large percentage of the total number of specimens. In particular, the standard deviation of the compressive strength for the innermost $0°$ ply-initiated fracture type was larger than that for the fixed-section fracture type although the average compressive strengths for each fracture type were similar. This suggests that the compressive strength of the innermost $0°$ ply is an important factor affecting the fracture behavior of the thick quasi-isotropic CFRP laminates.

3.3. Fracture surface observation

As shown in the high-speed images, the primary origin of the compressive fracture of the quasi-isotropic CFRP laminates was the micro damage of the innermost $0°$ ply of the specimen. The fractured specimen was observed using an optical microscope VHX-600 (Keyence Corp.) to investigate the mechanism of the initial fracture in the $0°$ ply. Fig. 9 shows the micrography around the initial fracture area in the free edge of the specimen. As shown in

10

Fig. 9(a), numerous fiber fracture in the 0° ply and interlaminar delamination can be observed. In addition, the initial fracture surface of the 0° ply is slanted against a horizontal plane as shown in Fig. 9(b), similar to the kink band fracture.

The initial fracture surface was observed using a scanning electron microscope (SEM) JSM-6010PLUS/LV (JEOL Ltd.), as shown in Fig. 10. In Fig. 10, the vertical direction of the figures coincides with the thickness direction of the specimen. The characteristic fracture surface of the fibers, comprising of clearly divided rough and smooth areas, can be observed, as shown in Fig. 10. This is the typical fracture surface generated by the microbuckling of the fibers. Fig. 11 is the schematic diagram of the relation between the series of the shear kinking and the generated fracture surface of the fibers. It has been reported that the microbuckling of the fibers occurs owing to an initial imperfection of the fiber orientation and shear deformation under a compressive load in the fiber direction [3]. As shown in Fig. 11(b), bending deformation occurs owing to the shear stress. Subsequently, the kink band failure and the tensile crack proceed from the compressive and tensile region on the surface of the fibers. Consequently, the smooth and rough fracture surfaces are generated by the compressive and tensile stresses. Therefore, the initial fracture of the 0° ply is the microbuckling of the fibers caused by the bending deformation in the thickness direction of the specimen.

3.4. FE analysis of shear stress distribution in 0° ply

As mentioned in the previous subsection, it was revealed that the origin of the compressive fracture of the quasi-isotropic CFRP specimen was the microbuckling in the 0° ply, which was due to shear deformation. The high-

11

speed images exhibited that such an initial fracture often occurred in the innermost $0°$ ply of the specimen. Therefore, the shear stress distribution in the $0°$ ply on the free edge was investigated using finite element (FE) analysis.

The FE model is shown in Fig. 12. In the model, the half area of the specimen in the thickness direction is considered because the stacking sequence is symmetric. The length, width, and thickness of the model are 100.0, 25.0, and 6.4, respectively, and each ply is divided by one layer of elements with the thickness of 0.2. The model is discretized into eight-node first-order isoparametric elements and the numbers of nodes and elements are 38115 and 34560, respectively. The elastic moduli of T800S/#3900-2B unidirectional CFRP laminates are shown in Table 3 [29]. Here, the subscripts L and T indicate the fiber longitudinal and transverse directions of the unidirectional laminates, and the L–T plane was rotated to correspond with the fiber longitudinal direction of each ply. The nodal displacement in the X-direction is -0.5 (0.5% compressive strain) at the upper surface and that of the lower surface is specified to zero. In addition, the Z-direction displacement is fixed at the surface of symmetry, i.e., the mid-plane of the specimen, and the fixed sections in the other surface.

The distributions of the out-of-plane shear stress τ_{ZX} at the free edge ($Y = 25.0$) and the center ($Y = 12.5$) at the gage section of the specimen are indicated in Fig. 13. Here, it is noted that the stress distributions are qualitative because the effects of stress singularity and plastic deformation around the interlaminar areas are neglected. As shown in the figures, a considerable shear stress occurs at the free edge of the specimen while the

stress is almost zero at the internal area. The numerical results obtained in this study agree with the previous studies in that the microbuckling tends to occur around the free edges of the specimen [20, 21, 22]. Fig. 14 shows the variation of the shear stress τ_{ZX} in the 0° plies at the center of the free edge. The shear stress increases by approximately 20% at the innermost 0° ply compared with the other 0° plies. This is the primary reason why the initial fracture in the 0° ply tends to occur near the mid-plane of the specimen.

Therefore, the series of compressive fracture mechanisms of the thick quasi-isotropic CFRP laminates was clarified. The out-of-plane shear stress occurred in the 0° ply of the quasi-isotropic CFRP laminates subjected to a compressive load. Such a shear stress increased at the innermost 0° ply and caused the initial fracture, which was the microbuckling of the fibers, at the innermost 0° ply of the specimen. Subsequently, a crack was generated from the initial fracture and propagated to the outer plies on one side of the specimen. Furthermore, the other side of the specimen began to fracture and finally the specimen fractured completely.

4. Conclusion

In the present study, the compressive fracture aspect for the thick quasi-isotropic CFRP laminates was investigated using a high-speed camera to clarify the progress of the brooming fracture. For the compressive tests, the alternative test fixture was developed to capture high-speed images. From the captured images, the fracture types of the 64-ply quasi-isotropic CFRP specimen were classified broadly into two groups based on the initial fracture points, the innermost 0° ply or the fixed sections of the specimen. The stan-

13

dard deviation of the compressive strength for the innermost 0° ply-initiated fracture type was larger than that for the fixed-section fracture type although the average compressive strengths for each fracture type were similar. Fractography confirmed that the initial fracture of the innermost 0° ply was due to the microbuckling of the fibers. An FE analysis was performed to investigate the stress distribution on the 0° plies of the specimen. The numerical results demonstrated a considerable out-of-plane shear stress around the free edges of the specimen, especially for the innermost 0° ply. Such a shear stress is thought to cause the microbuckling at the innermost 0° ply. Thereafter, the generated crack propagated to the outer plies on one side of the specimen, followed by propagating on the other side until the specimen was completely fractured. Therefore, the compressive strength of the innermost 0° ply was an important factor affecting the fracture behavior of the thick quasi-isotropic CFRP laminates.

Acknowledgements

References

[1] B. Budiansky, N.A. Fleck, Compressive failure of fibre composites, J. Mech. Phys. Solids 41 (1993) 183–211. https://doi.org/10.1016/0022-5096(93)90068-Q

[2] P. Berbinau, C. Soutis, I.A. Guz, Compressive failure of 0° unidirectional carbon-fibre-reinforced plastic (CFRP) laminates by fibre microbuckling, Compos. Sci. Technol. 59 (1999) 1451–1455. https://doi.org/10.1016/S0266-3538(98)00181-X

[3] A. Jumahat, C. Soutis, F.R. Jones, A. Hodzic, Fracture mechanisms and failure analysis of carbon fibre/toughened epoxy composites subjected to compressive loading, Compos. Struct. 92 (2010) 295–305. https://doi.org/10.1016/j.compstruct.2009.08.010

[4] A. Jumahat, C. Soutis, A. Hodzic, A graphical method predicting the compressive strength of toughened unidirectional composite laminates, Appl. Compos. Mater. 18 (2011) 65–83. https://doi.org/10.1007/s10443-010-9149-8

[5] T. Yokozeki, T. Ogasawara, T. Ishikawa, Effects of fiber nonlinear properties on the compressive strength prediction of unidirectional carbon-fiber composites, Compos. Sci. Technol. 65 (2005) 2140–2147. https://doi.org/10.1016/j.compscitech.2005.05.005

[6] T. Yokozeki, T. Ogasawara, T. Ishikawa, Nonlinear behavior and compressive strength of unidirectional and multidirectional carbon fiber composite laminates, Compos. Pt. A-Appl. S. Manuf. 37 (2006) 2069–2079. https://doi.org/10.1016/j.compositesa.2005.12.004

[7] A. Yoshimura, R. Hosoya, J. Koyanagi, T. Ogasawara, X-ray computed tomography used to measure fiber orientation

in CFRP laminates, Adv. Compos. Mater. 25 (2016) 19–30. https://doi.org/10.1080/09243046.2014.959240

[8] S.C. Garcea, Y. Wang, P.J. Withers, X-ray computed tomography of polymer composites, Compos. Sci. Technol. 156 (2018) 305–319. https://doi.org/10.1016/j.compscitech.2017.10.023

[9] D. Wilhelmsson, L.E. Asp, A high resolution method for characterisation of fibre misalignment angles in composites, Compos. Sci. Technol. 165 (2018) 214–221. https://doi.org/10.1016/j.compscitech.2018.07.002

[10] M.J. Emerson, Y. Wang, P.J. Withers, K. Conradsen, A.B. Dahl, V.A. Dahl, Quantifying fibre reorientation during axial compression of a composite through time-lapse X-ray imaging and individual fibre tracking, Compos. Sci. Technol. 168 (2018) 47–54. https://doi.org/10.1016/j.compscitech.2018.08.028

[11] K. Iizuka, M. Ueda, T. Takahashi, A. Yoshimura, M. Nakayama, Development of a three-dimensional finite element model for a unidirectional carbon fiber reinforced plastic based on X-ray computed tomography images and the numerical simulation on compression, Adv. Compos. Mater. 28 (2019) 73–85. https://doi.org/10.1080/09243046.2018.1434731

[12] I.M. Daniel, H.M. Hsiao, S.C. Wooh, Failure mechanisms in thick composites under compressive loading, Compos. Pt. B-Eng. 27 (1996) 543–552. https://doi.org/10.1016/1359-8368(95)00010-0

[13] J. Lee, C. Soutis, Thickness effect on the compressive strength of T800/924C carbon fibre-epoxy laminates,

Compos. Pt. A-Appl. Sci. Manuf. 36 (2005) 213–227. https://doi.org/10.1016/j.compositesa.2004.06.010

[14] E.M. Odom, D.F. Adams, Failure modes of unidirectional carbon/epoxy composite compression specimens, Compos. 21 (1990) 289–296. https://doi.org/10.1016/0010-4361(90)90343-U

[15] D. Purslow, Matrix fractography of fibre-reinforced epoxy composites, Compos. 17 (1986) 289–303. https://doi.org/10.1016/0010-4361(86)90746-9

[16] D. Purslow, Matrix fractography of fibre-reinforced thermoplastics, Part 1. Peel failures. Compos. 18 (1987) 365–374. https://doi.org/10.1016/0010-4361(87)90360-0

[17] D. Purslow, Matrix fractography of fibre-reinforced thermoplastics, Part 2. Shear failures, Compos. 19 (1988) 115–126. https://doi.org/10.1016/0010-4361(88)90721-5

[18] D. Purslow, Matrix fractography of fibre-reinforced thermoplastics, Part 3. Tensile, compressive and flexural failures, Compos. 19 (1988) 358–366. https://doi.org/10.1016/0010-4361(88)90123-1

[19] L. Shikhmanter, B. Cina, I. Eldror, Fractography of multidirectional CFRP composites tested statically, Compos. 22 (1991) 437–444. https://doi.org/10.1016/0010-4361(91)90201-Q

[20] H.T. Hahn, J.G. Williams, Compression failure mechanisms in unidirectional composites, in: J.M. Whitney, Composite Materials: Test-

ing and Design (Seventh Conference), ASTM International, West Conshohocken, PA, 2001, pp. 115–139. https://doi.org/10.1520/STP35345S

[21] M. Ueda, K. Mimura, T.K. Jeong, In situ observation of kink-band formation in a unidirectional carbon fiber reinforced plastic by X-ray computed tomography imaging, Adv. Compos. Mater. 25 (2016) 31–43. https://doi.org/10.1080/09243046.2014.973173

[22] Y. Wang, Y. Chai, C. Soutis, P.J. Withers, Evolution of kink bands in a notched unidirectional carbon fibre-epoxy composite under four-point bending, Compos. Sci. Technol. 172 (2019) 143–152. https://doi.org/10.1016/j.compscitech.2019.01.014

[23] ASTM Standard D3410-03, Standard test method for compressive properties of polymer matrix composite materials with unsupported gage section by shear loading, ASTM International, West Conshohocken, PA, 2003. https://doi.org/10.1520/D3410_D3410M-03

[24] SACMA Recommended Method 1R-94, Compressive properties of oriented fiber-resin composites, Suppliers of Advanced Composite Materials Association, Arlington, VA, 1994.

[25] ASTM Standard D695-02, Standard test method for compressive properties of rigid plastics, ASTM International, West Conshohocken, PA, 2002. https://doi.org/10.1520/D0695-02

[26] ASTM Standard D6641-01, Standard test method for compressive properties of polymer matrix composite materials using a combined load-

ing compression (CLC) test fixture, ASTM International, West Conshohocken, PA, 2001. https://doi.org/10.1520/D6641_D6641M-01E01

[27] T. Ogasawara, T. Ishikawa, A simple test method, NAL-II, to evaluate the strength and elastic modulus of polymer matrix composite laminates, Adv. Compos. Mater. 25 (2016) 131–145. https://doi.org/10.1080/09243046.2016.1226689

[28] H. Kusano, Y. Aoki, Y. Hirano, Y. Nagao, The fracture observation of a unidirectional CFRP by high speed imaging. J. Jpn. Soc. Compos. Mater. 37 (2011) 63–69 (in Japanese). https://doi.org/10.6089/jscm.37.63

[29] T. Morimoto, S. Sugimoto, H. Kato, E. Hara, T. Yasuoka, Y. Iwahori, T. Ogasawara, S. Ito, JAXA Advanced Composites Database, Japan Aerospace Exploration Agency, 2018 (in Japanese). https://repository.exst.jaxa.jp/dspace/handle/a-is/874006

Table 1: Young's modulus, compressive strength and fracture strain of 64-ply quasi-isotropic CFRP specimens.

Number of specimens	44
Young's modulus [GPa]	52.6 (1.2)
Compressive strength [MPa]	605.6 (27.1)
Fracture strain [%]	1.30 (0.09)

( ) indicates standard deviation

Table 2: Fracture types related to Young's modulus, compressive strength and fracture strain of 64-ply quasi-isotropic CFRP specimens.

	Type-A	Type-B	Type-C
Number of specimens	1	16	6
Young's modulus [GPa]	51.9 (−)	53.1 (1.5)	51.7 (0.4)
Compressive strength [MPa]	599.6 (−)	601.4 (31.9)	612.3 (16.1)
Fracture strain [%]	1.35 (−)	1.27 (0.10)	1.30 (0.10)

( ) indicates standard deviation

Table 3: Elastic moduli of T800S/#3900-2B unidirectional CFRP laminates [29].

Young's modulus	E_L [GPa]	153.0
	E_T [GPa]	8.0
Shear modulus	G_{LT} [GPa]	4.03
Poisson's ratio	ν_{LT}	0.34
	ν_{TT}	0.45

Figure 1: Brooming fracture mode for quasi-isotropic CFRP laminates under compressive load.
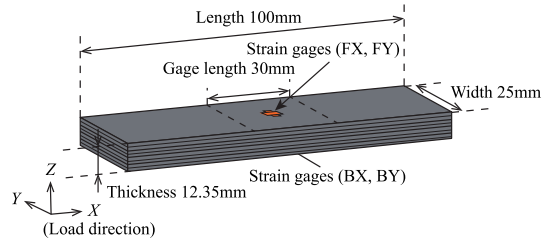
Figure 2: Specimen geometry for compressive tests.
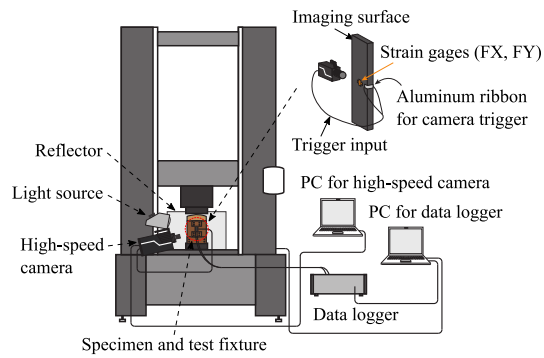
Figure 3: Compressive test system.
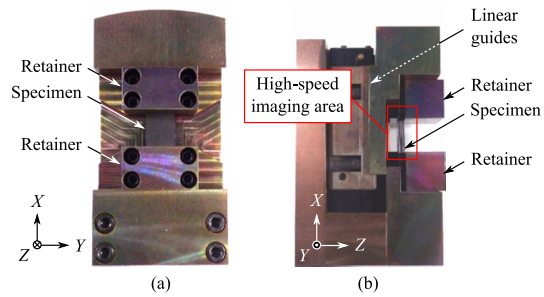
Figure 4: Compressive test fixture; (a) front and (b) side views.

23
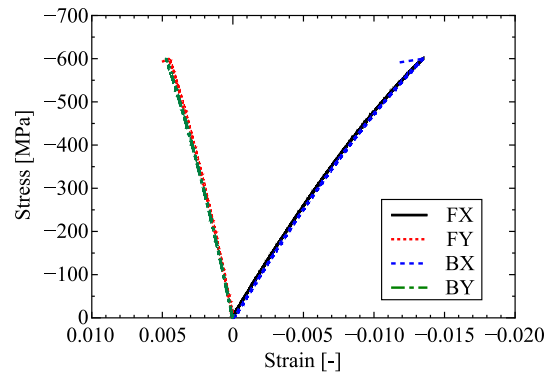
Figure 5: Representative stress-strain curves of quasi-isotropic CFRP specimen.
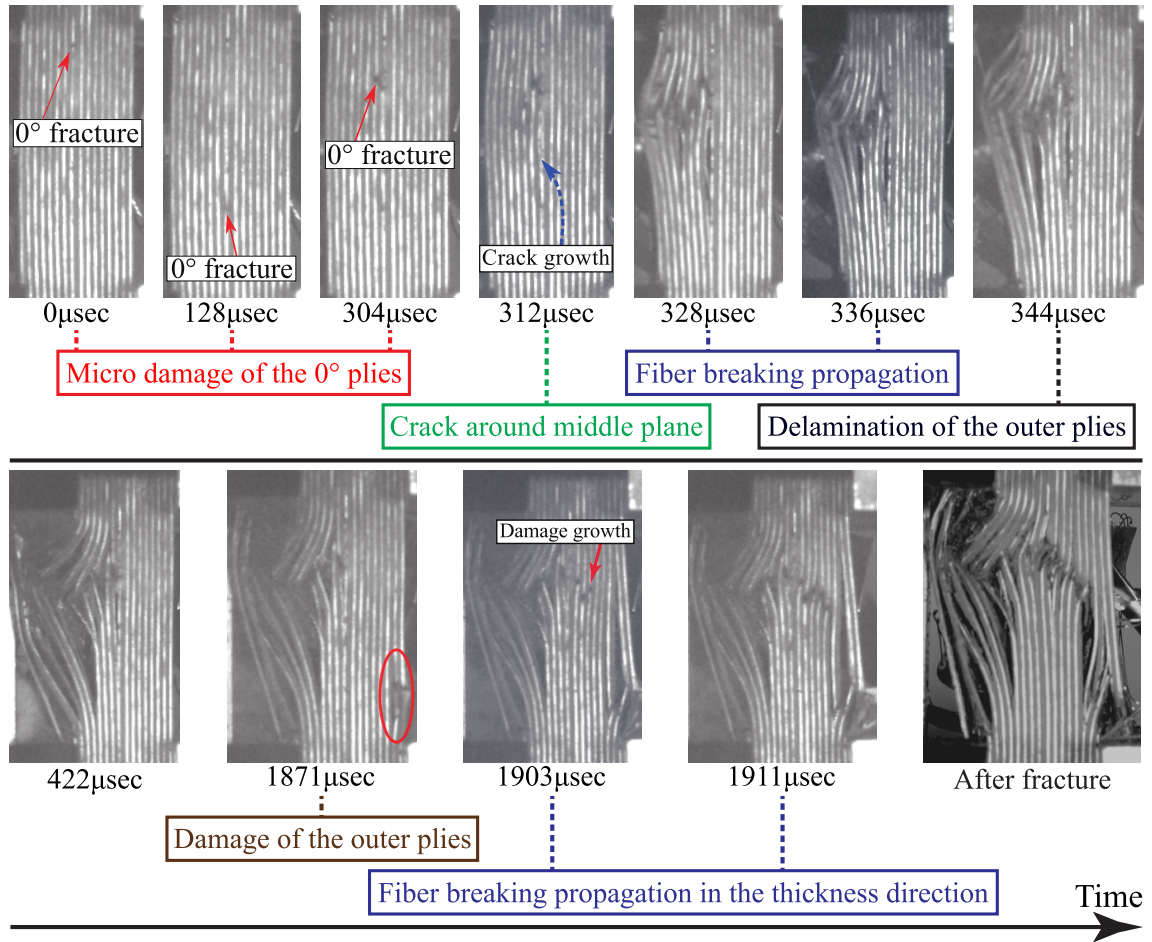
Figure 6: History of type-A compressive fracture.
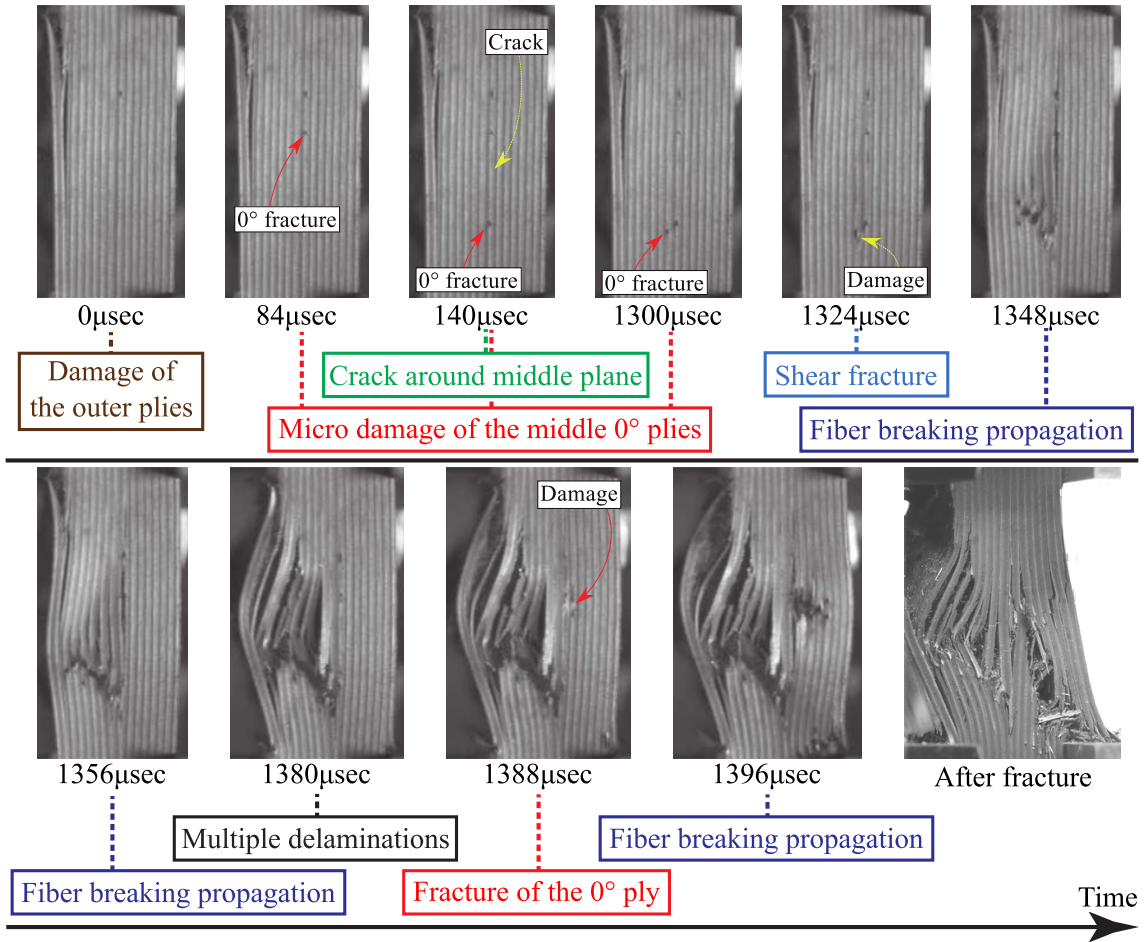
Figure 7: History of type-B compressive fracture.
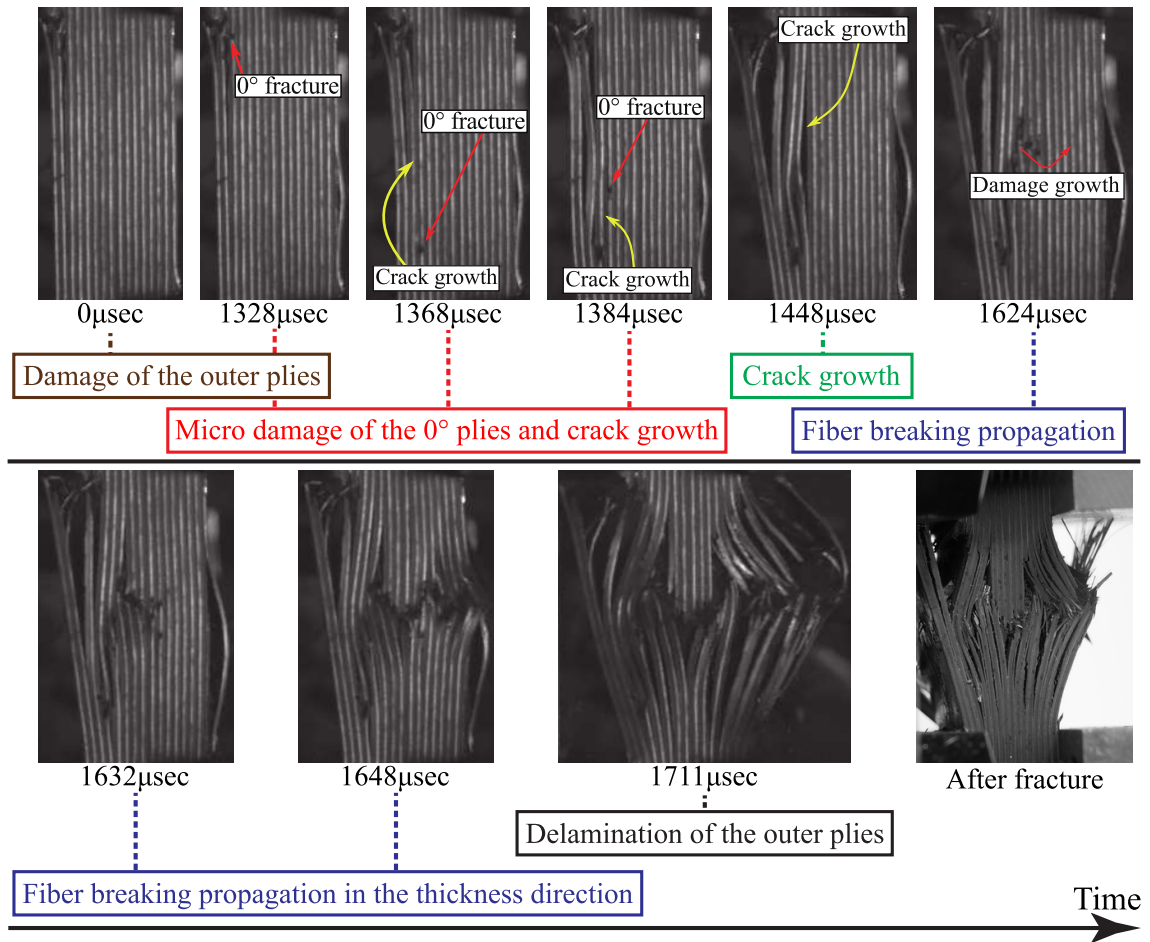
Figure 8: History of type-C compressive fracture.
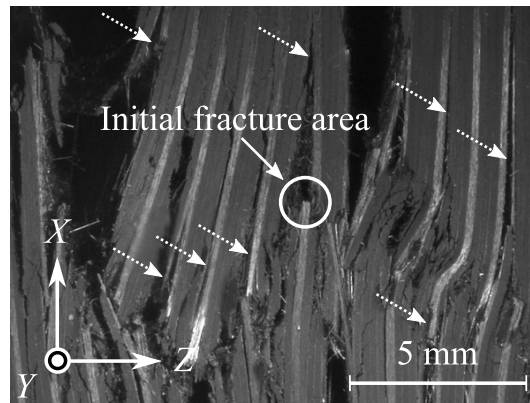
(a)
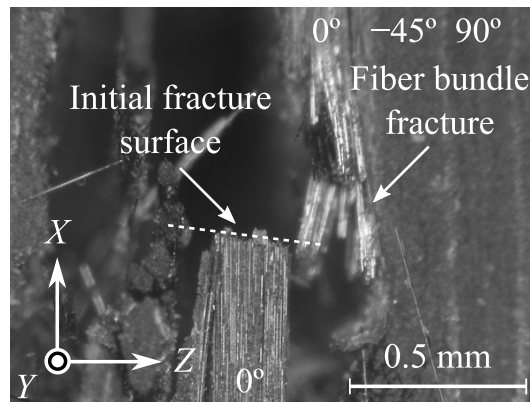
(b)

Figure 9: Optical microscope images after compressive fracture (a) at free edge of specimen and (b) around initial fracture surface.
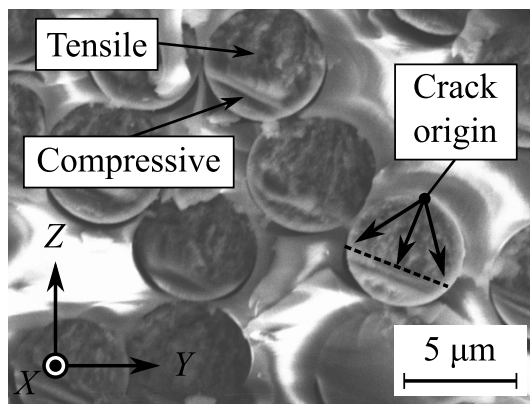
Figure 10: SEM image of initial fracture surface in 0° ply under compressive load.
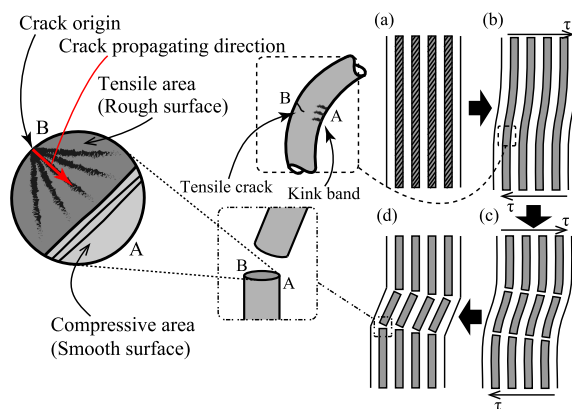
Figure 11: Schematic diagram of relation between shear kinking and fracture surface of carbon fiber.
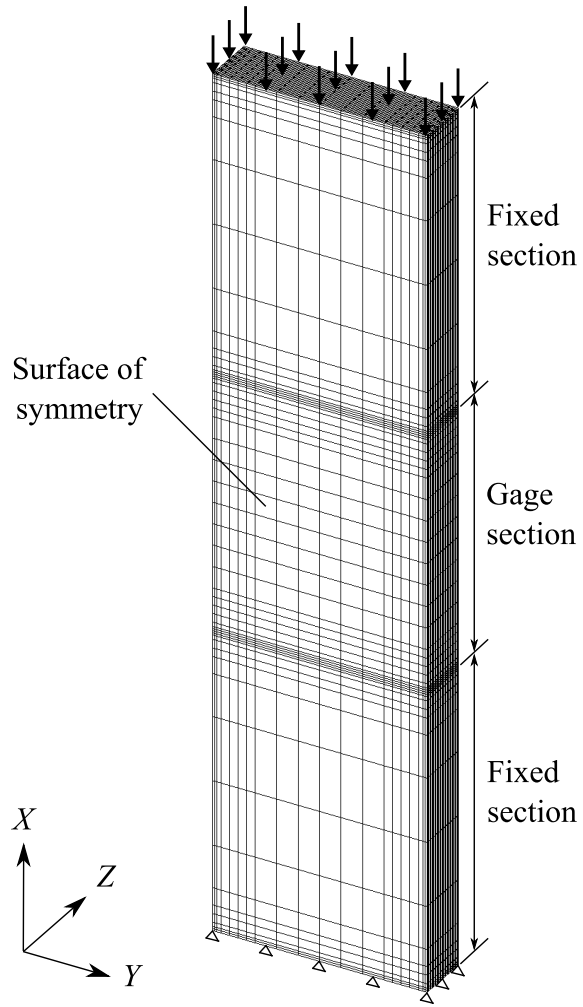
Figure 12: FE model for 64-ply quasi-isotropic CFRP specimen.
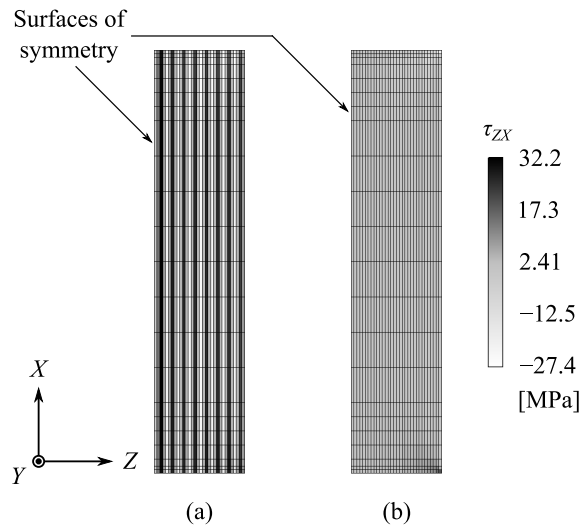
Figure 13: Distribution of shear stress τ_{ZX}; (a) free edge ($Y = 25.0$) and (b) center ($Y = 12.5$) at gage section of specimen.
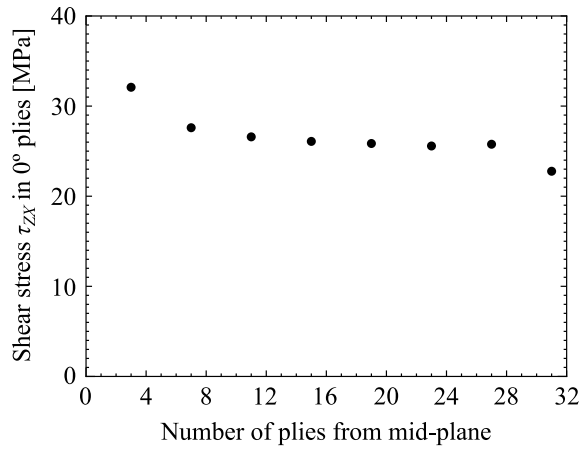

Figure 14: Distribution of shear stress τ_{ZX} in $0°$ plies at free edge of specimen.